



This is a repository copy of *Mitigation of unbalanced magnetic force in a PM machine with asymmetric winding by inserting auxiliary slots.*

White Rose Research Online URL for this paper:  
<http://eprints.whiterose.ac.uk/139347/>

Version: Accepted Version

---

**Article:**

Ma, J. and Zhu, Z.Q. [orcid.org/0000-0001-7175-3307](https://orcid.org/0000-0001-7175-3307) (2018) Mitigation of unbalanced magnetic force in a PM machine with asymmetric winding by inserting auxiliary slots. IEEE Transactions on Industry Applications, 54 (5). pp. 4133-4146. ISSN 0093-9994

<https://doi.org/10.1109/TIA.2018.2829879>

---

© IEEE 2018. Personal use of this material is permitted. Permission from IEEE must be obtained for all other users, including reprinting/ republishing this material for advertising or promotional purposes, creating new collective works for resale or redistribution to servers or lists, or reuse of any copyrighted components of this work in other works. Reproduced in accordance with the publisher's self-archiving policy.  
[http://www.ieee.org/publications\\_standards/publications/rights/rights\\_policies.html](http://www.ieee.org/publications_standards/publications/rights/rights_policies.html)

**Reuse**

Items deposited in White Rose Research Online are protected by copyright, with all rights reserved unless indicated otherwise. They may be downloaded and/or printed for private study, or other acts as permitted by national copyright laws. The publisher or other rights holders may allow further reproduction and re-use of the full text version. This is indicated by the licence information on the White Rose Research Online record for the item.

**Takedown**

If you consider content in White Rose Research Online to be in breach of UK law, please notify us by emailing [eprints@whiterose.ac.uk](mailto:eprints@whiterose.ac.uk) including the URL of the record and the reason for the withdrawal request.



[eprints@whiterose.ac.uk](mailto:eprints@whiterose.ac.uk)  
<https://eprints.whiterose.ac.uk/>

# Mitigation of Unbalanced Magnetic Force in PM Machine with Asymmetric Winding by Inserting Auxiliary Slots

Jie Ma, and Z. Q. Zhu, Fellow, IEEE

**Abstract**— Permanent magnet machine has received much attention recently. However, unbalanced magnetic force (UMF) may occur in PM machines with some slot/pole number combinations even there is no rotor eccentricity, which can cause high vibration and noise. In order to reduce the rated on-load UMF, three 3-slot/2-pole PM machines with different auxiliary slots are investigated and compared in this paper. In the first two machines, namely Machine 1 and Machine 2, the auxiliary slots are inserted in the middle of stator teeth, while their sizes are optimized under different working conditions, i.e. no-load and rated on-load conditions. In contrast, both position and size of auxiliary slots are optimized under rated on-load condition in the third machine, viz. Machine 3. Comparing with the conventional prototype machine, the maximum rated on-load UMFs are reduced by 6.3%, 50.7% and 96.6%, and the rated output torques are decreased by 0.7%, 11.5% and 4% in these three machines, respectively. In addition, the other electromagnetic performance, such as flux linkage, back EMF, cogging torque, rated output torque and torque ripple are compared. The influence of working conditions is investigated, and the experiments are also carried out to validate the numerically predicted results.

**Index Terms**—3-slot/2-pole, auxiliary slots, permanent magnet machine, unbalanced magnetic force.

## I. INTRODUCTION

PERMANENT magnet (PM) machines have received much attention recently due to their high efficiency, high torque density and high power factor [1], [2]. However, due to the asymmetric stator topology and unbalanced winding distribution, UMF occurs both under no-load and on-load conditions in machines with specific slot/pole combinations [3], which can cause high vibration as well as noise, and significantly reduce the life of bearings.

Many paper have investigated the UMF. The production mechanism of UMF was given in [4], it shows that the two field harmonics differed by one could result in the UMF. The UMFs in machines with axial even and axial-varying eccentricity were calculated by analytical method in [5], [6]. [7] and [8] used a 2-D conformal mapping method to calculate the UMF caused by eccentricity in surface mounted PM machines. The difference of UMF between internal and external fractional-slot PM machine was studied in [9]. [10]-[12] compared the UMF

in surface-mounted permeant magnet (SMPM) machines having different slot/pole combinations, and the influence of design parameters on UMF was investigated in [13]-[15].

The reduction of UMF has also been widely investigated for decades. Various methods have been proposed which can be classified as machine control methods and machine design optimizations [16]. As for the machine control methods, field weakening commutation strategy can be used to minimize on-load UMF [17]. A similar method is introduced in [18] which injected appropriate current to compensate the low order spatial harmonics of air-gap flux density. An effective method of rotor optimization is shaping and magnetizing magnets properly [19], [20]. In [21], another method is proposed by adding notches in the rotor of interior permeant magnet machines. However, these methods lead to complex machining process which increases the cost significantly. The shaped rotor may have mechanical problem when it runs under high-speed condition [22]. In addition to rotor shape optimization, UMF can be also reduced by stator structure optimization. In [23], the no-load UMF is decreased by adding auxiliary slots into the middle of stator teeth with the same size comparing with slot openings. However, this method has very limited influence on the rated on-load UMF. Different types of auxiliary slots were used in [24], which shows auxiliary slots with optimal size and position has the best performance as for rated on-load UMF reduction.

The aim of this paper is to compare the electromagnetic performance of several machines with different auxiliary slots, with emphasis on the maximum rated on-load UMF reduction. Although there are many different slot/pole combinations, the 3-slot/2-pole machine is chosen at first due to the simple rotor and stator structure. The feasibility of the proposed method on other slot/pole combinations will be validated in later part.

This paper is organized as follow, in Section II, the 2D model of a conventional 3-slot/2-pole PM prototype machine is introduced and its UMF characteristics are analyzed. In Section III, the UMFs of machines with different auxiliary slots are investigated, and their other electromagnetic performances are compared in Section IV. In Section V, the effect of working conditions are investigated. The influence of slot/pole combinations and magnetizations on effectiveness of proposed method is investigated in Section VI. Finally, the experiments are carried out to validate the numerically predicted results.

## II. UMF OF CONVENTIONAL 3-SLOT/2-POLE MACHINES

The cross section of a conventional 3-slot/2-pole PM prototype machine is shown in Fig. 1, and its detailed parameters are listed in Table I. In the prototype machine, the concentrated winding and a 2-pole PM ring are employed.

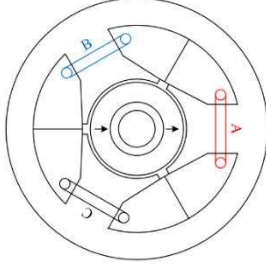


Fig. 1. Cross section of prototype 3-slot/2-pole PM machine.

TABLE I  
BASIC PARAMETERS OF MACHINE

Slot number	3	Shaft diameter (mm)	7
Pole number	2	Magnet thickness (mm)	4
Stator outer diameter (mm)	50	Axial length (mm)	30
Stator inner diameter (mm)	19	Magnet remanence (T)	1.2
Stator yoke height (mm)	5.2	Rated current (A)	10
Slot opening (mm)	2	Current angle (Elec. Deg.)	0
Air-gap length (mm)	0.6	Rated speed (rpm)	1000
Rotor outer diameter (mm)	18	Number of turns per phase	32

To obtain the characteristics of UMF, the field distribution needs to be investigated at first as the UMF origins essentially from the asymmetric magnetic field distribution. The no-load and on-load field distributions are shown in Fig. 2. It is found that the field is symmetrical along the x-axis at this rotor position under no-load condition, which means there is only x-axis direction component of UMF. However, the field is modified when the currents are input, armature field makes the on-load field not symmetrical along the x-axis anymore, and hence there will be an extra UMF component in y-axis which does not only affect the amplitude but also the phase of total UMF.

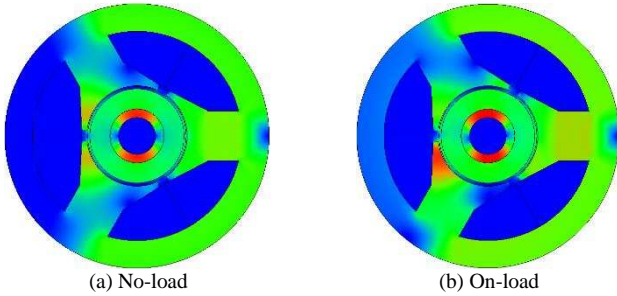


Fig. 2. No-load and rated on-load field distributions of a conventional 3-slot/2-pole PM machine at 0s.

By way of example, the comparison of UMF under no-load and on-load conditions is shown in Fig. 3. It is found that the amplitude of UMF is significantly increased by input current. Meanwhile, the phase of on-load UMF lags behind the no-load one about 90 degrees, which confirms that a measurable y-axis UMF component is introduced due to the enhancement of armature field.

Since both PM field and armature field have great influence on the on-load UMF, the on-load UMF has to be decomposed according to the source so that the contribution of each

magnetic fields can be studied in details.

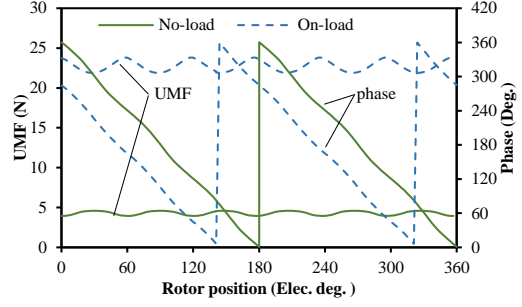


Fig. 3. UMF comparison between no-load and on-load condition of conventional 3-slot/2-pole machine.

The UMF based on the Maxwell stress tensor can be calculated by [15]

$$F_x = r l_a \int_0^{2\pi} (\sigma \cdot \cos \alpha + \tau \cdot \sin \alpha) d\alpha \quad (1)$$

$$F_y = r l_a \int_0^{2\pi} (\sigma \cdot \sin \alpha - \tau \cdot \cos \alpha) d\alpha \quad (2)$$

where  $F_x$  and  $F_y$  are UMF components in x and y directions,  $r$  is the radial of middle of air-gap,  $\alpha$  is the rotor position in mechanical degree,  $l_a$  is the active length of machine,  $\sigma$  and  $\tau$  are the radial and circumferential traveling stresses, respectively, which can be calculated by

$$\sigma = \frac{B_r^2 - B_t^2}{2\mu_0} \quad (3)$$

$$\tau = \frac{B_r \cdot B_t}{\mu_0} \quad (4)$$

where  $B_r$  and  $B_t$  are the radial and tangential components of air-gap flux density, which can be expressed as

$$B_r = B_{mr} + B_{ar} \quad (5)$$

$$B_t = B_{mt} + B_{at} \quad (6)$$

where  $B_{mr}$ ,  $B_{ar}$  and  $B_{mt}$ ,  $B_{at}$  are the radial and tangential flux densities of PM and armature fields. Since both these two field components are affected by saturation, the frozen permeability method is used here for separating the flux densities [25], which could be calculated as follows: at a specific working condition, the permeability distributions of soft magnetic material under on-load condition can be predicted and saved by finite element method. Then the PM field is calculated by setting current as zero and employing the permeability distributions just obtained. By this means, the PM field considering the influence of armature field on saturation can be predicted precisely. Following the same procedure, the corresponding armature field can be also calculated. It should be noticed that while calculating  $B_{ar}$  and  $B_{at}$ , the remanence of magnet material should be set as zero, but the relative permeability of magnet should not be changed. In this way, the radial and tangential travelling stresses can be decomposed as:

$$\sigma = \underbrace{\frac{\sigma_1}{2\mu_0}}_{\sigma_1} + \underbrace{\frac{\sigma_2}{2\mu_0}}_{\sigma_2} + \underbrace{\frac{\sigma_3}{\mu_0}}_{\sigma_3} \quad (7)$$

$$\tau = \underbrace{\frac{\tau_1}{\mu_0}}_{\tau_1} + \underbrace{\frac{\tau_2}{\mu_0}}_{\tau_2} + \underbrace{\frac{\tau_3}{\mu_0}}_{\tau_3} \quad (8)$$

where  $\sigma_1, \tau_1, \sigma_2, \tau_2$  and  $\sigma_3, \tau_3$  are the radial and tangential traveling stresses caused by the self-interaction of PM field, the self-interaction of armature field, and the mutual interaction between these two fields, respectively. The UMF caused by the self-interaction of PM field introduces UMF under the open-circuit condition, and the UMF caused by the interaction between the armature field and the PM field aggravates the UMF under on-load situation. For convenience, F1 and F2 are used here to represent these two components which resulted from  $\sigma_1, \tau_1, \sigma_2, \tau_2$ . Although the self-interaction of armature field can also affect unbalanced magnetic force, its value is far lower comparing with the other two UMF components due to the large equivalent airgap length caused by relative thick magnet thickness, and therefore this part of UMF is neglected in following analysis.

For instance, the amplitude and phase of F1 and F2 are calculated and shown in Fig. 4, it can be seen that F1 has great difference comparing with no-load UMF no matter as for amplitude or phase shown in Fig. 3, even if both of them are caused by the self-interaction of PM field. In order to explain this phenomenon, the PM field flux distributions under no-load and rated on-load conditions are shown in Fig. 5. As can be seen, the PM field flux distribution under rated on-load condition is not symmetrical along x-axis anymore which is due to the modified permeability distribution caused by armature field. Consequently, the phase difference between F1 and F2 is slightly bigger than 90 degree, and there is a small cancelling effect between F1 and F2.

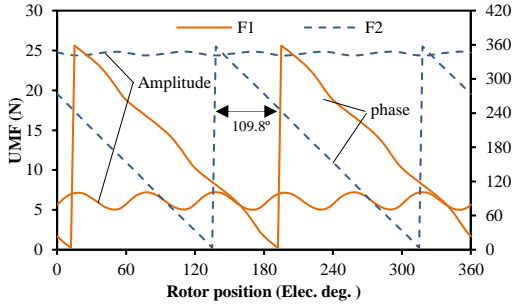


Fig. 4. Comparison of F1 and F2 of the conventional 3-slot/2-pole PM machine.

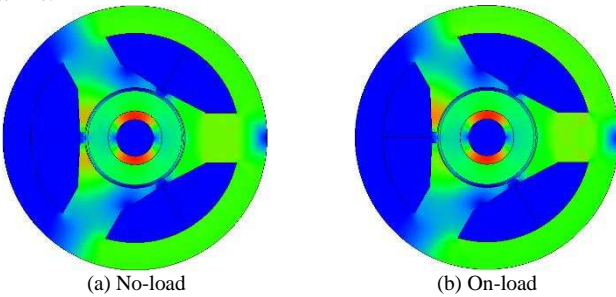


Fig. 5. No-load and rated on-load PM field distributions of a conventional 3-slot/2-pole PM machine at 0s.

### III. INVESTIGATION OF EFFECT OF AUXILIARY SLOTS ON UNBALANCED MAGNETIC FORCE MITIGATION

Since the main reason for no-load UMF is the asymmetric distributed slot openings rather than stator slots [23], the auxiliary slots with the same size as slot openings can be inserted into the middle of stator teeth to balance the slot

opening distribution, and no-load UMF can be almost eliminated by this means.

However, due to the fact that F2 is much higher comparing with F1 as shown in last section, the rated on-load UMF is just slightly reduced by this method since the reduction is mainly achieved by reducing F1. In other words, the optimization goal of this method is the minimum no-load UMF instead of the minimum rated on-load UMF.

Alternatively, the optimization goal can be changed to the minimum rated on-load UMF. As a result, the size of auxiliary slots could be modified significantly. By way of example, the topologies of these two machines, namely Machine 1 and Machine 2, are shown in Fig. 6, whose optimization goals are the minimum no-load and rated on-load UMFs, respectively. The optimization of Machine 2 is carried out by FE method, both height and width of auxiliary slots have been optimized. The detailed parameters of their auxiliary slots are listed in Table II. It can be seen that Machine 2 has much larger auxiliary slots comparing with Machine 1.

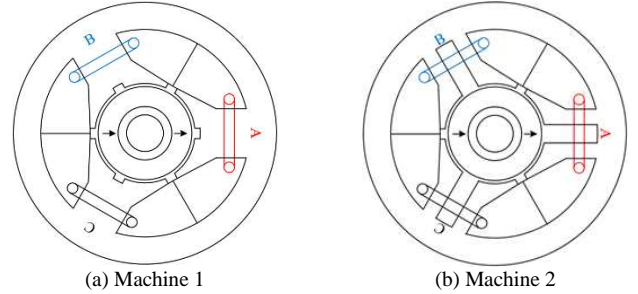


Fig. 6. Optimized topologies of Machine 1 and Machine 2.

TABLE II  
SPECIFICATION COMPARISON

Parameters	Machine 1	Machine 2
Auxiliary slot opening width (mm)	2	3.5
Auxiliary slot opening height (mm)	1	10.1

Fig. 7 compares their performance on UMFs. It should be mentioned that the auxiliary slots change not only the air-gap permeance distribution but also the saturation of stator, i.e. stator tooth body. Therefore, both F1 and F2 are affected by auxiliary slots. As a result, F1' and F2' are employed here to represent those two UMF components considering the influence of auxiliary slots.

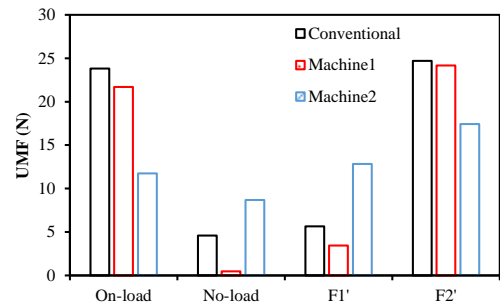
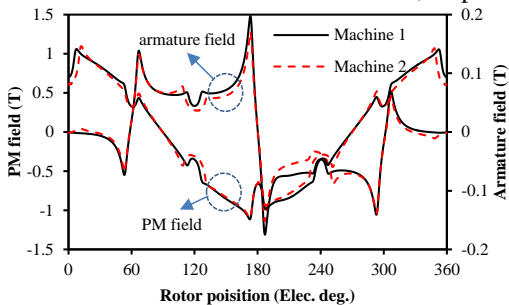


Fig. 7. Comparison of maximum value of UMFs.

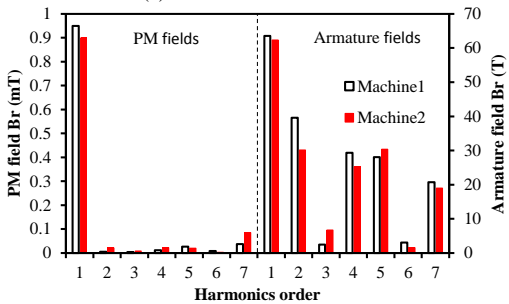
As shown in Fig. 7, both Machine 1 and Machine 2 can reduce the rated on-load UMF, but the reduction of Machine 1 is much lower than Machine 2, which is due to different functions of auxiliary slots in these two machine. In Machine 1,

the auxiliary slots is mainly for balancing the slot opening distributions, hence the asymmetric air-gap permeance variation. However, the main function of auxiliary slots in Machine 2 is reducing the harmonics content of armature field and fundamental PM field, which is achieved by larger equivalent air-gap length.

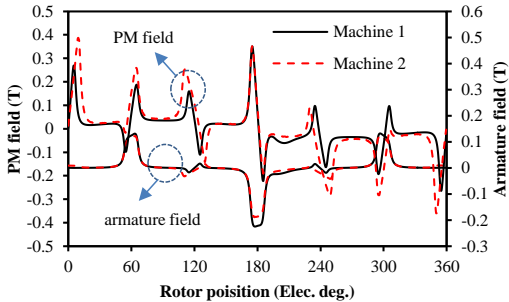
By way of examples, the field distributions of Machine 1 and Machine 2 are calculated by the frozen permeability method and shown in Fig. 8. Due to the fact that the UMF is resulted from any two adjacent field harmonics, although there are abundant harmonic contents, according to (1) to (10), the main part of  $F1'$  and  $F2'$  origins from the interaction between the fundamental PM radial field and the 2<sup>nd</sup> PM tangential harmonic as well as the 2<sup>nd</sup> armature harmonic, respectively.



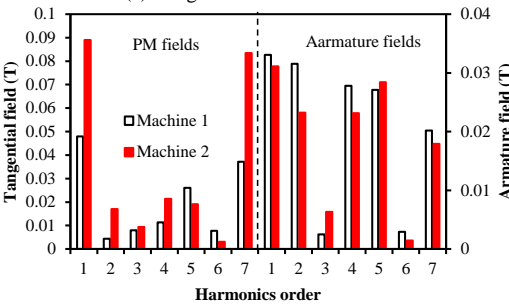
(a) Radial field waveforms



(b) Radial field spectra



(c) Tangential field waveforms



(d) Tangential field spectra

Fig. 8. Comparison of PM and armature fields of Machine 1 and Machine 2.

It can be seen that the harmonic content of PM field of Machine 1 is much lower comparing with Machine 2, especially the 2<sup>nd</sup> tangential harmonic, which results in lower  $F1'$ . However, the harmonics content of armature field of Machine 1 is much higher which makes the  $F2'$  of Machine 1 is larger than Machine 2. In contrast, the armature field harmonics as well as fundamental PM field are lower in Machine 2. As a consequence, Machine 2 has relative larger  $F1'$  but lower  $F2'$ .

Since  $F1$  is caused by the self-interaction of PM field, its phase mainly depends on the saturation condition and rotor position. From another perspective, if the rotor position and load condition are treated as fixed, the phase of  $F1$  can be seen as a function of the position of the slot openings. As the auxiliary slots have almost the same function as the conventional slots on no-load UMF, this rule can be also applied to auxiliary slots. Since the amplitude of  $F1'$  can be adjusted by modifying the size of auxiliary slots, and its phase can be modified by shifting its position, it is possible to make  $F1'$  and  $F2'$  have the same amplitude but opposite direction by using auxiliary slots with optimized size and position, and hence the on-load UMF can be eliminated by this means.

The parameters of auxiliary slots used in this method are shown in Fig. 9, where  $s_o$  and  $d_{s_o}$  are the width of slots and auxiliary slots, respectively.  $s_d$ ,  $d_{s_d}$  are the height of slots and auxiliary slots, and  $\alpha$  is the shift angle of auxiliary slots.

The Machine 3 represents the machine optimized by this method, the FE method is employed for global optimization, and it is optimized under rated on-load condition. The optimized variables are  $d_{s_o}$ ,  $d_{s_d}$  as well as  $\alpha$ , and the optimization goal is the minimum rated on-load UMF. However, it should be noticed that the existence of auxiliary slots can result in torque reduction due to the increased equivalent airgap length, while significant torque decrease is usually unacceptable in practice. As a result, only the candidates of which the torque decrease is smaller than 5% will be considered further, and the machine having minimum rated on-load UMF among the qualified candidates will be chosen as the optimal one. The cross section of the optimal topology is shown in Fig. 10, and the parameters of auxiliary slots of Machine 3 are listed in Table III.

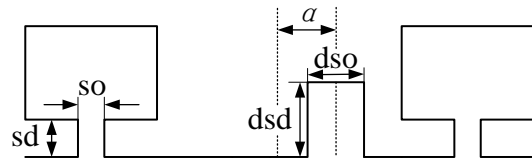


Fig. 9. Auxiliary slots with shift angle.

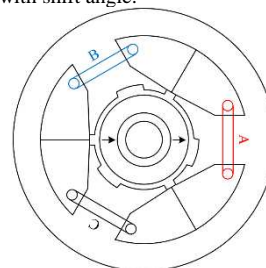


Fig. 10. Cross section of Machine 3.

TABLE III  
SPECIFICATION COMPARISON

Parameters	Machine 3
Slot opening width (mm)	2
Slot opening height (mm)	1
Auxiliary slot opening width (mm)	4.98
Auxiliary slot opening height (mm)	0.98
Auxiliary slots shift angle (deg.)	14.18

Fig. 11 compares the maximum UMFs of Machine 3 under different input currents. It can be found that the proposed machine achieves almost zero UMF under rated on-load condition that current equals to 10A. This is due to the fact that F1' has the opposite phase and almost the same amplitude comparing with F2' under this condition. Except for rated on-load condition, the UMF of the Machine 3 is not zero anymore due to the variation of armature field and the modified permeability distribution. In contrast, the UMF of the conventional machine increases over the whole current range due to the fact that the phase between F1 and F2 is close to 90 degrees. Consequently, F1 and F2 have very small cancelling effect comparing with Machine 3.

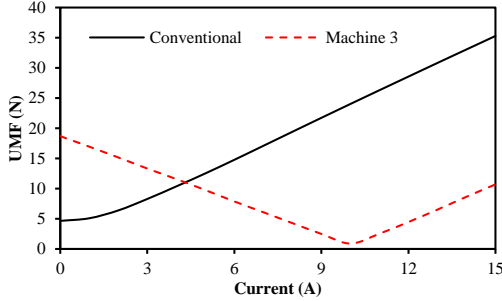


Fig. 11. Comparison of maximum UMFs of conventional machine and Machine 3 under different working conditions.

The rated on-load UMF is 0.8N in the Machine 3 but 23.8N in the conventional one, the reduction is about 96.6%, which shows the great effectiveness of this method. It is worth noting that F2' highly depends on working load conditions. Therefore, F1' needs to be modified according to different input currents to obtain low UMF. As a result, the optimal size and position of auxiliary slots vary with working conditions as shown in Fig. 12.

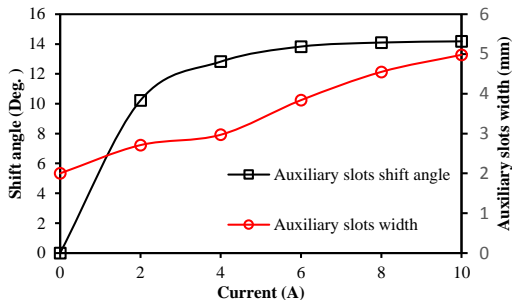


Fig. 12. Optimal shift angle and width of auxiliary slots for minimum UMF with different currents.

In order to illustrate the working mechanism of the proposed method, a simple magnetomotive force (MMF)-permeance model is introduced.

The MMF of the PM field could be expressed as:

$$F_{PM}(\theta, t) = F_{PM} \cdot \cos(\theta - \omega t) \quad (9)$$

where  $\theta$  indicates the rotor position in electrical angle and the  $\omega$  is the electrical angular speed. Since the parallel magnetization is used in the prototype machine, there is no harmonics in MMF distribution.

The airgap permeance model accounting for conventional stator slots is shown in Fig.13 and it can be decomposed into a series of Fourier series as:

$$P(\theta) = P_0 + P_{kn_r} \sum_{k=1}^{\infty} \cos(kn_r (\theta - \theta_0)) \quad (10)$$

where  $P_0$  and  $P_{kn_r}$  are the coefficients of DC and harmonic components of permeance,  $k$  is the index of each harmonic,  $n_r$  is the number of stator tooth and  $\theta_0$  indicates the phase difference.

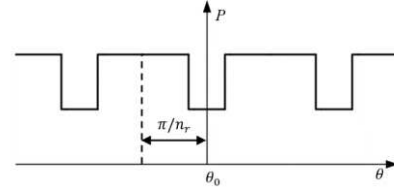


Fig. 13. Airgap permeance distributions accounting for stator slots.

As a result, the open-circuit airgap flux density could be calculated by multiplying the MMF of PM field as well as airgap permeance distributions.

$$\begin{cases} B_{PM}(\theta, t) = F_{PM}(\theta, t) \cdot P(\theta) \\ = P_0 F_{PM} \cdot \cos(\theta - \omega t) + \frac{1}{2} F_{PM} P_{kn_r} \sum_{k=1}^{\infty} (\cos A + \cos B) \\ A = (kn_r + 1)\theta - kn_r \theta_0 - \omega t \\ B = (kn_r - 1)\theta - kn_r \theta_0 + \omega t \end{cases} \quad (11)$$

As can be seen, the abundant slot harmonics can be introduced, and adjacent harmonics appear due to asymmetric stator structure which results in no-load UMF.

Since the auxiliary slots have almost same function in terms of modifying airgap permeance distribution, (9)-(11) could also be used for calculating the slot harmonics produced by auxiliary slots, the design parameters  $d_{so}$  and  $d_{sd}$  determine the coefficient of permeance distribution and the shift angle  $\alpha$  affects the phase. Consequently, the auxiliary slots with optimal size and position significantly change the amplitude and phase of slot harmonics, and it is possible that utilizing the slot harmonics to compensate the other even order airgap flux density harmonics under rated working condition. By this means, the rated on-load UMF could be greatly reduced.

It should be noticed that the MMF-permeance model is only for illustration instead of giving the precise solution of each design parameter. This is due to the fact that the auxiliary slots also have significant influence on saturation distribution, especially the local saturation, which has great influence on airgap permeance distribution. Since the saturation could not be considered in analytical method, the direct solution of the analytical model will have significant error comparing with the optimal solution. As a result, the FE method will still be used for later investigation.

To show more detail, F1' and F2' in Machine 3 against auxiliary slots shift angle are shown in Fig. 14. The rated current is 10A and current angle is 0 electrical degree. It can be

seen that the position of auxiliary slots has a great effect on  $F1'$  for both phase and amplitude. In contrast,  $F2'$  is much less sensitive as for the position of auxiliary slots. This is due to the fact that  $F1'$  is caused by the self-interaction of PM field, in which all harmonics except the fundamental are caused by slotting effect, and therefore the permeance variation affected by auxiliary slots has great impact on the PM field harmonics in addition to the fundamental. As for the fundamental of PM field, its amplitude and phase are related to the equivalent air-gap length and the initial position of rotor, respectively. Hence, the auxiliary slots can only decrease its amplitude but have very small effect on its phase. On the contrary,  $F2'$  is mainly caused by the fundamental harmonic of PM field and the second harmonic of armature field [12], and the armature field harmonics are mainly originated from the armature field instead of slot harmonics. Therefore, the auxiliary slots have the similar influence on armature field comparing with the fundamental of PM field.

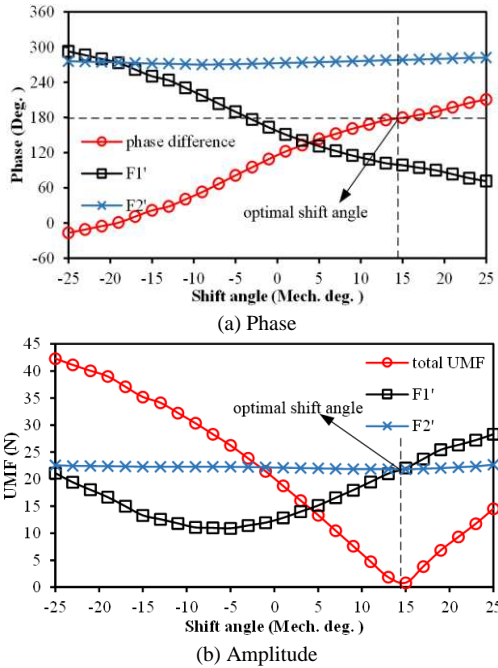


Fig. 14.  $F1'$  and  $F2'$  versus auxiliary slots shift angle at 0s.

By way of example, the harmonics in PM field and armature field with different shift angles are shown in Fig. 15. It is worth mentioning that since the fundamental PM field is very insensitive to the shift angle of auxiliary slots, and its value is much larger than the other harmonics, it is not shown here so that the other harmonics can be observed more clearly.

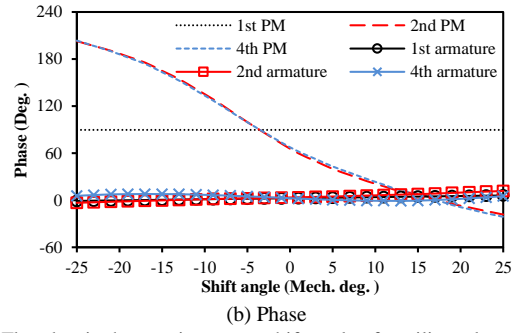
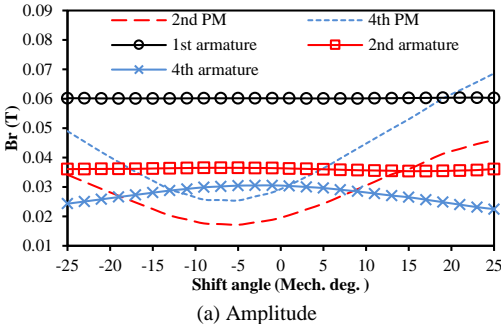


Fig. 15. Flux density harmonics versus shift angle of auxiliary slots.

#### IV. MACHINE PERFORMANCE

In previous sections, three 3-slot/2-pole PM machines with different auxiliary slots are presented, and their UMFs are compared in detail. In this section, their other electromagnetic performance are evaluated and compared.

##### A. Flux-linkage and Back EMF

Fig. 16 shows the comparison of phase flux linkages. It is found that Machine 1 and Machine 3 have almost same phase flux linkage comparing with the conventional one, the slight reduction is mainly due to the increased airgap length caused by auxiliary slots. In contrast, flux linkage in Machine 2 is much lower, which is mainly due to the much larger auxiliary slots, hence the larger equivalent air-gap length.

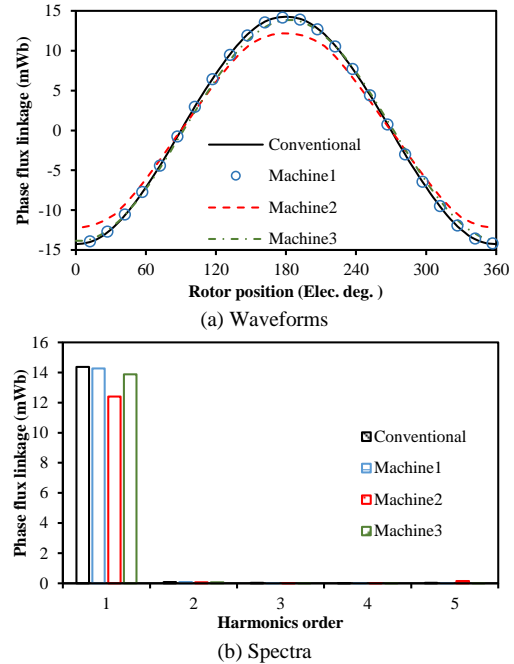


Fig. 16. Phase flux linkage comparison.

The phase back electromagnetic forces (EMF) are compared in Fig. 17.

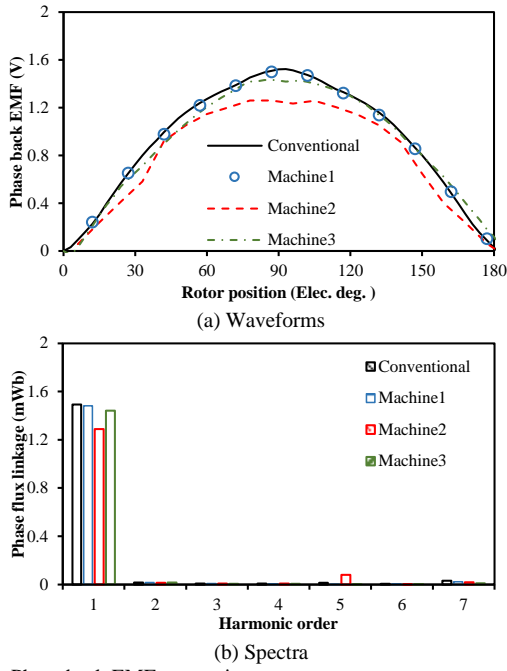


Fig. 17. Phase back EMF comparison.

Since the back EMF is proportional to the phase flux linkage, the auxiliary slots have the similar effect on back EMF comparing with flux linkage. Consequently, the fundamental back EMFs present the same trend comparing with flux linkages.

In terms of the harmonics content, all of the machines have a very sinusoidal waveform expect for Machine 2 in which the 5th harmonic is more measurable comparing with other machines. As a result, the torque ripple of Machine 2 is aggravated.

### B. Cogging Torque

Fig. 18 compares the cogging torques. It can be seen that Machine 1 has the lowest cogging torque which is due to the balanced air-gap permeance distribution caused by auxiliary slots. Moreover, the difference between the conventional machine, Machine 1 and Machine 3 is very small. In contrast, the cogging torque of Machine 2 is much higher, which is mainly caused by the much larger auxiliary slots.

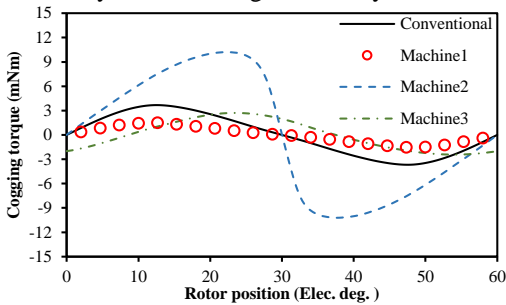


Fig. 18. Cogging torque comparison.

### C. On-load Torque

In addition, the on-load torques are simulated and shown in Fig. 19. It is found that since the auxiliary slots are very small, there is only very slight difference between the conventional machine and Machine 1. However, auxiliary slots have more

significant effect on Machine 2 and Machine 3. Since the auxiliary slots increase the equivalent air-gap length much more significantly comparing with Machine 1, the reduction of rated on-load torque in Machine 2 and Machine 3 is more measurable. In addition, the saturation in Machine 2 is more heavier due to the thinner tooth width. Consequently, the Machine 2 has the lowest output torque. The rated output torques are decreased by 0.7%, 11.5% and 4% in three machines, respectively.

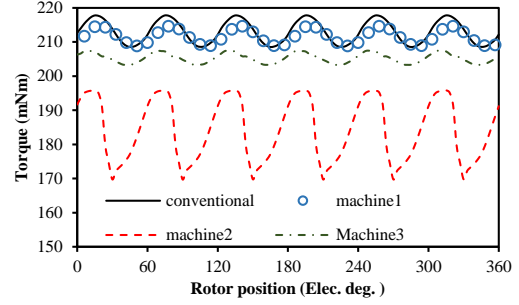


Fig. 19. On-load torque comparison.

The comparison of rated on-load torque ripple is shown in Table IV. It shows the difference between Machine 1, Machine 3 and the conventional machine is very small, the slight reduction is mainly due to the mitigation of cogging torque. In contrast, Machine 2 has the largest torque ripple which is due to the increased cogging torque and the relative measurable back EMF harmonics.

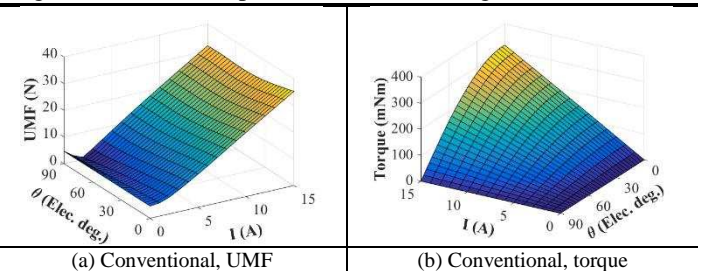
TABLE IV  
TORQUE RIPPLE COMPARISON

Machine name	Torque ripple (mNm)
Conventional	9.27
Machine1	5.81
Machine2	26.14
Machine3	4.20

### V. EFFECT OF WORKING CONDITIONS

Previous sections investigated the performance of three machines with different auxiliary slots under rated working conditions according to the maximum torque per ampere (MTPA) control strategy. Since the machine mostly operates under rated working condition in various applications, e.g. vacuum cleaner, etc. The best performance under rated working condition is the most important. However, the load may change in few situations. Therefore, the effect of working conditions is also important which will be investigated in this section.

The maximum on-load UMFs and average torques of three machines with different working conditions are shown in Fig.20, in which  $\theta$  represents the current angle.



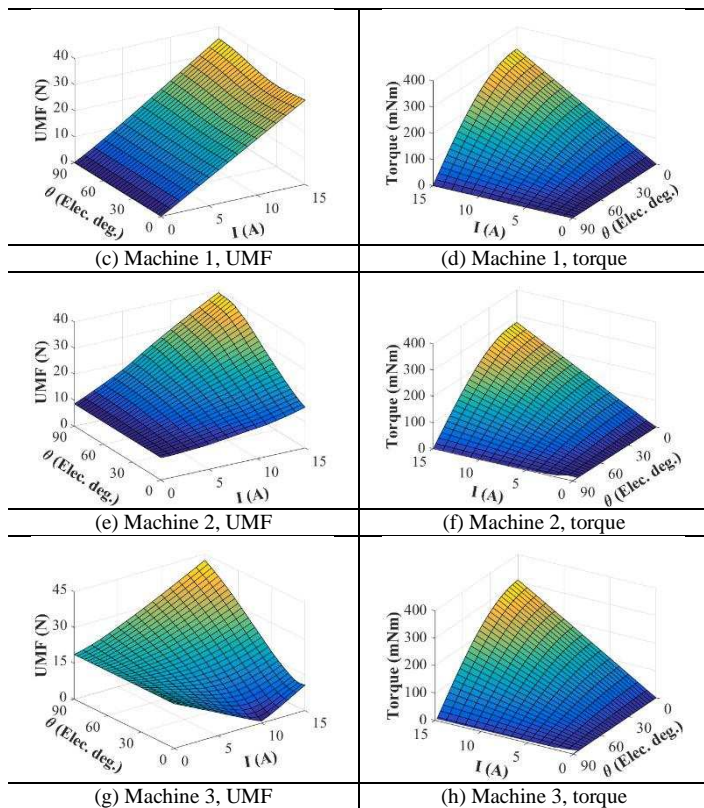


Fig. 20. Performance of machines against different working conditions.

It can be found that all of the machines have similar torque characteristics which are proportional to current amplitude but inversely proportional to current angle. However, since the on-load torque is inversely proportional to the equivalent air-gap length affected by auxiliary slots, Machine 2 has the lowest on-load torque and the conventional one has the highest on-load torque. It is worth noting that the Machine 1 has the almost same characteristics as the conventional machine, this is due to the auxiliary slots in Machine 1 are very small, as a result, they have negligible influence on the equivalent airgap length as well as tooth saturation.

As for maximum UMFs, four machines have very different behaviour. It can be seen that the maximum UMF is proportional to current amplitude but almost irrelevant to current angle in the conventional machine. This is due to the slot openings are too small to affect UMF notably, and F2 dominates the value of on-load UMF. As the same reason, the Machine 1 has very similar characteristics as the conventional one when the current is relative high. However, Machine 1 has very low UMF when the current is small, this is due to the F1' dominates the whole value of UMF in this condition, and the F1' is very small in Machine 1 due to the balanced airgap permeance distribution. In contrast, auxiliary slots have significant influence on Machine 2 and Machine 3. In Machine 2, the phase difference between F1' and F2' is reduced gradually with the increasing of current angle, and the additive effect makes on-load UMF increase significantly. In contrast, Machine 3 can almost eliminate the UMF on rated working condition, and the reason has been detailed in Section III. However, it should be noticed that since the proposed method

employed in Machine 3 is using the slot harmonics produced by the auxiliary slots to compensate other undesirable airgap flux density harmonics, it is very hard to make the machine optimized by the proposed method have better overall performance, which is due to the undesirable harmonics provided by armature field vary with different working conditions. Nevertheless, the proposed method could offer better performance in a relative range as shown in Fig. 20.

In addition, although both current amplitude and current angle can affect the on-load UMF of Machine 3 significantly, but the reasons are different. The influence of current amplitude is investigated at first. By way of example, the field distributions of machines with different input currents, i.e. 2A, 10A and 15A, are given in Fig. 21, and the UMF components with different current amplitudes are shown in Fig. 22.

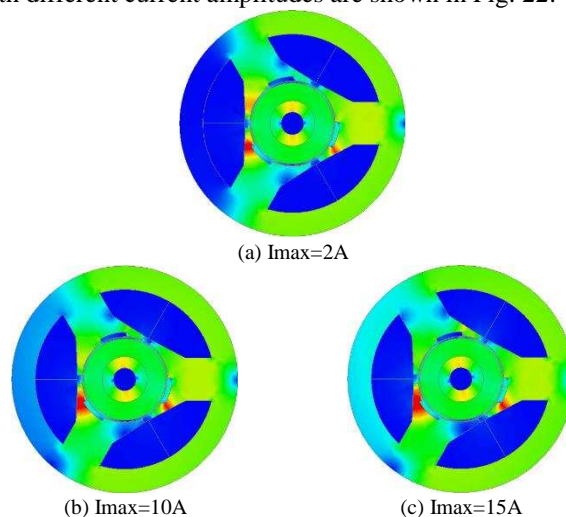
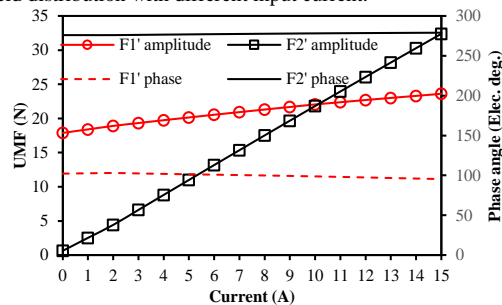


Fig. 21. Field distribution with different input current.

Fig. 22.  $F1'$  and  $F2'$  with different input current value at 0s.

It can be seen that the both  $F1'$  and  $F2'$  rise with the increase of input current. The increase of  $F1'$  is mainly due to the aggravated saturation and the growth of  $F2'$  is mainly caused by the improved armature field. As for their phase, since the rotor position and current angle are kept as the same, both of  $F1'$  and  $F2'$  remain the almost same phases during whole current interval.;

The influence of current angle on UMF is shown in Fig. 23 and Fig. 24.

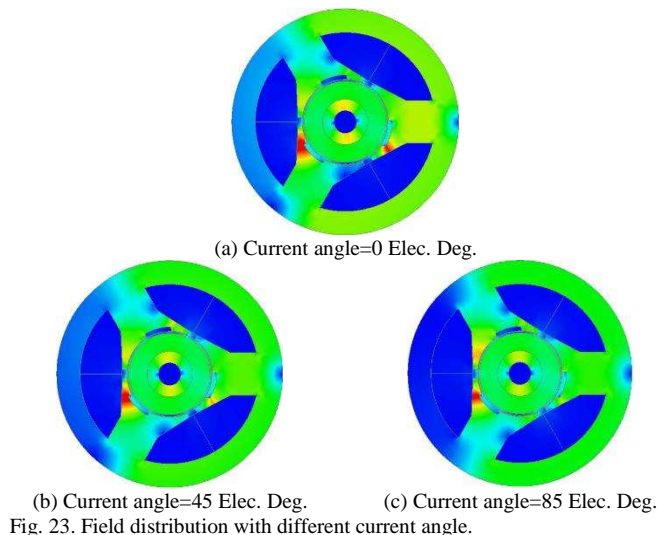
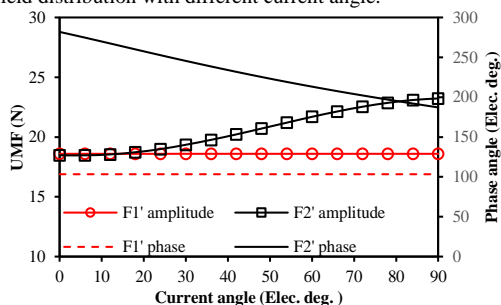


Fig. 23. Field distribution with different current angle.

Fig. 24.  $F1'$  and  $F2'$  with different current angle.

Different from the effect of current amplitude, the current angle has great impact on the phase of  $F2'$  which decreases from 270 degrees to 180 degrees linearly when current angle changes from 0 degree to 90 degrees. This is due to the fact that the phase of  $F2'$  is determined by the phase of armature field as well as PM field, since the phase of PM field is not changed, the phase of  $F2'$  is mainly decided by the phase of armature field, hence the current angle. As for the amplitude, both of  $F1'$  and  $F2'$  are affected which is due to the fact that the permeance distribution changes with the current angle as well.

## VI. INFLUENCE OF SLOT/POLE COMBINATIONS AND MAGNETIZATIONS

As shown above, the machine with optimal size and position of auxiliary slots can provide excellent performance of rated on-load UMF reduction. However, the previous sections are based on a simple and specific 3-slot/2-pole machine structure to ease the investigation and illustration. In this part, the feasibility of the proposed method on 9-slot/8-pole machines will be validated. It should be noted that the parallel magnetization is identical to Halbach magnetization in 2-pole machine, which indicates that there is no MMF harmonics in PM field. However, these two magnetizations will be different in machines with other pole numbers. Consequently, both 9-slot/8-pole machines having parallel and Halbach magnetizations will be investigated.

The cross sections of conventional and optimal machines are shown in Fig. 25 and the detailed parameters are shown in Table V and Table VI.

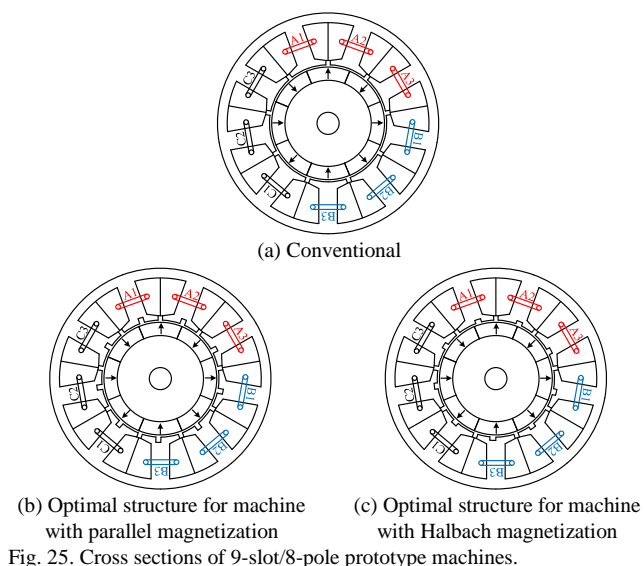


Fig. 25. Cross sections of 9-slot/8-pole prototype machines.

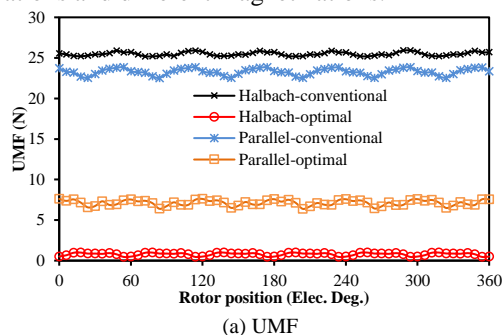
TABLE V  
BASIC PARAMETERS OF MACHINE

Slot number	9	Shaft diameter (mm)	7
Pole number	8	Magnet thickness (mm)	3
Stator outer diameter (mm)	50	Axial length (mm)	30
Stator inner diameter (mm)	26.5	Magnet remanence (T)	1.2
Stator yoke height (mm)	2.2	Rated current (A)	10
Slot opening (mm)	1	Current angle (Elec. Deg.)	0
Air-gap length (mm)	0.5	Rated speed (rpm)	1000
Rotor outer diameter (mm)	25.5	Number of turns per phase	33

TABLE VI  
SPECIFICATION COMPARISON

Parameters	Halbach array
Auxiliary slot opening width (mm)	1.36
Auxiliary slot opening height (mm)	0.74
Auxiliary slots shift angle (deg.)	2.89
Parameters	Parallel magnetization
Auxiliary slot opening width (mm)	1.14
Auxiliary slot opening height (mm)	1.20
Auxiliary slots shift angle (deg.)	1.87

The comparisons of rated on-load UMF and output torque are shown in Fig. 26. As can be seen, the proposed method can reduce as much as 96.2% and 68.7% of UMF and the torque reduction are 4.8% and 4.9% in machine with Halbach and parallel magnetizations. The results show the proposed method can also offer great effectiveness on other slot/pole combinations and different magnetizations.



(a) UMF

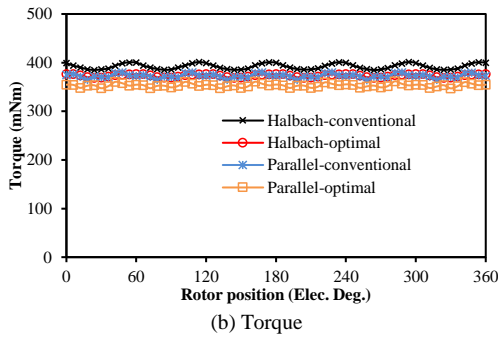


Fig. 26. Rated on-load UMF and torque comparison of 9-slot/8-pole machines with parallel and Halbach magnetizations.

It should be noticed that the machine with Halbach array can benefit more from the proposed method, which is due to two different reasons. Firstly, the parallel magnetization results in more abundant airgap flux density harmonics due to additional MMF harmonics. As a result, the machine with parallel magnetization also has significantly higher both no-load and on-load UMFs. In addition, the Halbach array can also provide higher 4<sup>th</sup> airgap flux density harmonic. According to (9)-(11), the required size of auxiliary slots in machine having Halbach array can be smaller and hence more considerable rated on-load UMF reduction when the torque reduction is limited as 5%.

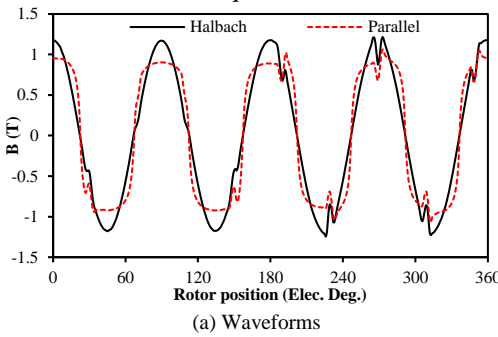


Fig. 27. Open circuit airgap flux density comparison of 9-slot/8-pole machines with parallel and Halbach magnetizations.

It should be noticed that the machine with parallel magnetization also could have extremely low rated on-load UMF by employing the proposed method when the output torque reduction is not limited. As shown in Fig. 28, the maximum reduction of rated on-load UMF can be as much as 93.4%, while the torque reduction is 15.8% in this situation.

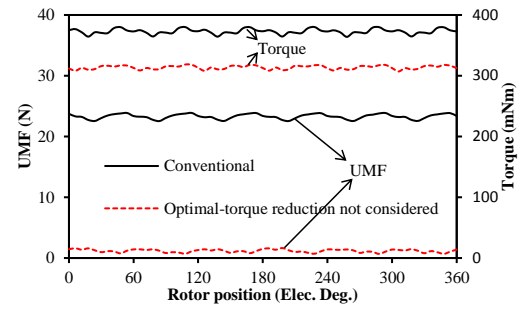


Fig. 28. Rated on-load UMF and torque comparison of 9-slot/8-pole machines with parallel magnetization.

## VII. EXPERIMENTAL VALIDATION

To validate the previous numerical analyses, three prototype machines are built, i.e., the conventional machine, Machine 2 and Machine 3. The detailed main design parameters are listed in previous sections. It should be noticed that the Machine 1 has not been built since it has very similar electromagnetic performance comparing with the conventional machine. Three prototype machines are shown in Fig. 29. All machines share the same rotor, in which the magnetic ring is used.

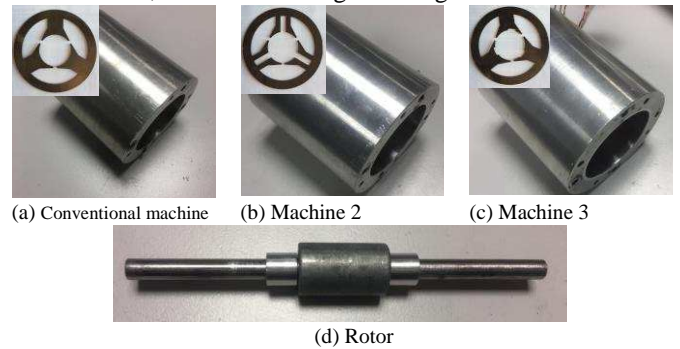
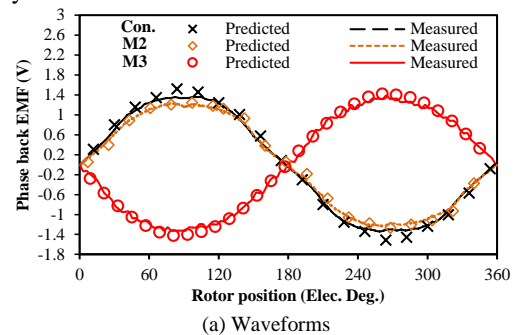


Fig. 29. Stators and rotor for the prototype 3-slot/2-pole machines.

The measured phase back EMFs with 1000 r/min are shown in Fig. 30 which have excellent agreements comparing with the predicted values. The slight difference is mainly due to the manufacture error as well as the end effect. Moreover, it is evident that the conventional machine has the highest phase back EMF, while the difference between Machine 3 and conventional machine is very small, the slight reduction is due to the increased equivalent airgap length caused by the auxiliary slots.



(a) Waveforms

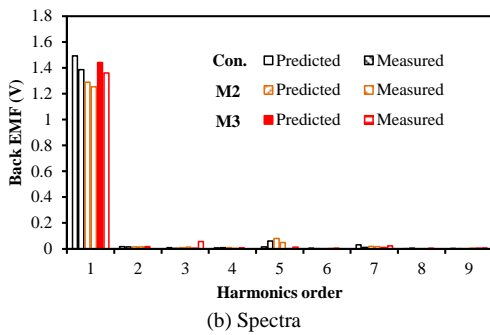


Fig. 30. Comparison of FE-predicted and measured back EMFs at 1000r/min.

In addition, the predicted and measured static torques with different rotor positions and currents are compared in Fig.31. Good agreements can be observed, while there is still slight error which is due to the tolerance in manufacturing and end effect. In addition, the test rig may also have influence on the measured value since the static torque is small and relative sensitive to the test environment.

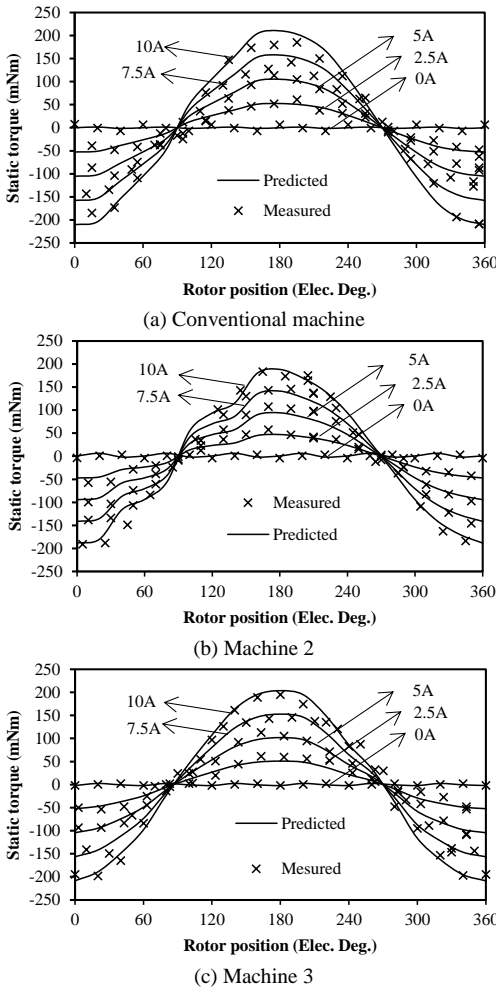


Fig. 31. Comparison of FE-predicted and measured static torques with different rotor positions and q-axis currents.

The UMFs are also tested. It should be noticed that it is very complicated to measure the variation of the UMF with different rotor positions. Instead, the UMF with one fixed rotor position is tested. As for the fixed rotor position, it is chosen as the position under zero d-axis current control for all machines,

which means the North Pole is always aligned with the Phase A.

It should be mentioned that the phase of maximum UMF changes with the input current, which means it is very hard to measure it directly even if the rotor is kept as the same position. However, it is possible to measure both the vertical and horizontal UMF components, and the resultant UMF can be obtained and observed by using interpolation method, which is shown in Fig.34. As a result, the special end cap needs to be used which is shown in Fig.32, the hole for shaft is deeper as much as 0.5mm for one side in the special end cap. By this means, the shaft can move from the normal position to an eccentric position.

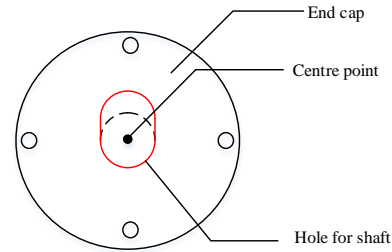


Fig. 32. Special end caps for UMF test.

The whole test rig is shown in Fig.33. As can be seen, the eccentric hole is upwards and a wire is used to connect the shaft holder and the counterweight. The windings in all three machines are excited with  $I_A = 0$  and  $I_B = -I_C = -\frac{\sqrt{3}}{2}I_{DC}$  for a q-axis current. When the gravity of the counterweight, rotor and shaft holder is balanced with the UMF in vertical direction, the shaft will be at normal position and any small force upwards will stabilize the rotor in the eccentric position.

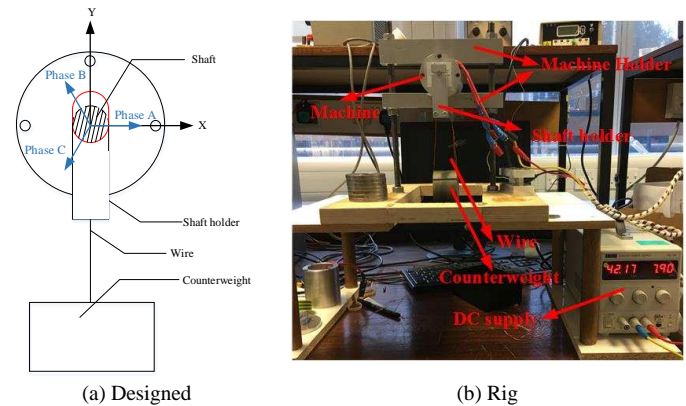


Fig. 33. Test rig UMF.

It should be noticed that since the UMFs have both vertical and horizontal components and their values could be positive and negative. As a result, the displacement of stator depends on the direction of the UMF components needed to be tested. The stator positions with different UMF components are listed in Table VII. In terms of the direction of UMF, the initial position of machine is located as shown in Fig. 33, which means  $F_x$  has the same phase with Phase A, and  $F_y$  is located in a direction of  $F_x$  counter clockwise ninety degrees.

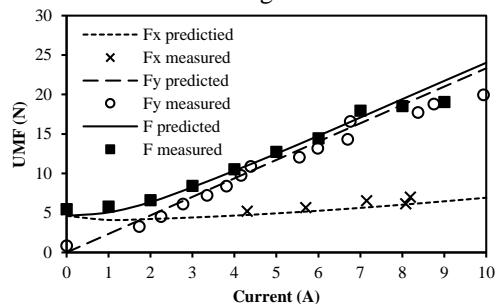
TABLE VII

STATOR DISPLACEMENT WITH DIFFERENT UMFs NEEDED TO BE TESTED

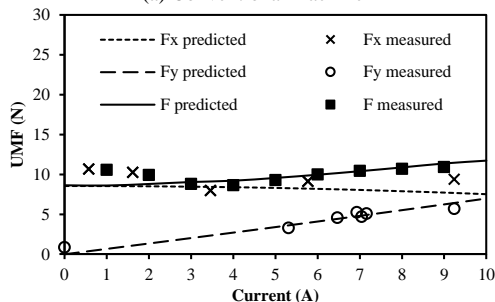
UMF components	$F_x$ Positive	$F_x$ Negative
Stator displacement		
UMF components	$F_y$ Positive	$F_y$ Negative
Stator displacement		

The comparison of predicted and measured UMFs are shown in Fig.34. Both the horizontal and vertical UMF components are tested. However, due to the fact that the mass of the counterweight is discrete, the resultant UMF is obtained by using interpolation method. As shown, the difference between predicted and measured values are small. The slight error may be caused by the frictional force, misalign between the North Pole and phase A as well as the manufacture tolerance.

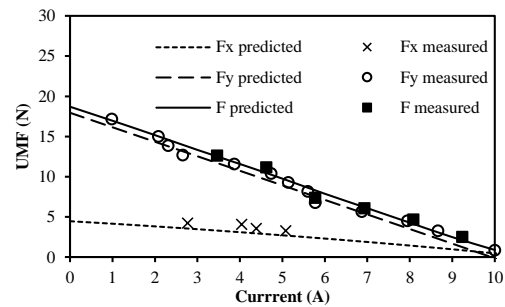
The experimental results also show that the Machine 3 has the lowest maximum rated on-load UMF while the conventional machine has the highest one.



(a) Conventional machine



(b) Machine 2



(c) Machine 3

Fig. 34 Comparison of FE-predicted and measured UMF at specific rotor positions;  $I_A = 0A$ , and  $I_B = -I_C = -\frac{\sqrt{3}}{2} I_{DC}$ .

## VIII. CONCLUSION

In this paper, the characteristics of UMF in conventional 3-slot/2-pole machine has been studied at first. Then, three machines with different type of auxiliary slots are investigated and compared. It shows that Machine 1 has the best performance as for no-load UMF reduction, but it has very limit reduction on rated on-load UMF. Both Machine 2 and Machine 3 can reduce the rated on-load UMF significantly, but Machine 3 can almost eliminated the rated on-load UMF. As for the output torque, both Machine 1 and Machine 3 have good performance, while the Machine 2 has a much lower output torque. However, Machine 3 also has some drawbacks and limitations, i.e. the output torque is decreased slightly and the performance of on-load UMF mitigation is highly depended on working conditions. Finally, the experiments are carried out to validate the numerical analyses results, which has good agreement with the predicted value.

## REFERENCES

- [1] D. Gerada, A. Mebarki, N. L. Brown, C. Gerada, A. Cavagnino, and A. Boglietti, "High-speed electrical machines: technologies, trends, and developments," *IEEE Trans. Ind. Electron.*, vol. 61, no. 6, pp. 2041-2059, 2014.
- [2] A. Tenconi, S. Vaschetto, and A. Vigliani, "Electrical machines for high-speed applications: design considerations and tradeoffs," *IEEE Trans. Ind. Electron.*, vol. 61, no. 6, pp. 3022-3039, 2014.
- [3] Z. Q. Zhu, D. Ishak, D. Howe, and J. Chen, "Unbalanced magnetic forces in permanent-magnet brushless machines with diametrically asymmetric phase windings," *IEEE Trans. Ind. Appl.*, vol. 43, no. 6, pp. 1544-1553, 2007.
- [4] Bi, C., Liu, Z.J., Low, T.S., "Analysis of unbalanced-magnetic-pulls in hard disk drive spindle motors using a hybrid method", *IEEE Trans. Magn.*, 1996, 32, (5), pp. 4308-4310.
- [5] Y. X. Li, Q. F. Lu, and Z. Q. Zhu, "Unbalanced magnetic force prediction in permanent magnet machines with rotor eccentricity by improved superposition method," *IET Electric Power Applications*, vol. 11, no. 6, 2017.
- [6] Y. X. Li, and Z. Q. Zhu, "Cogging torque and unbalanced magnetic force prediction in PM machines with axial-varying eccentricity by superposition method," *IEEE Trans. Magn.*, vol. 53, no. 11, 2017.
- [7] J. T. Li, Z. J. Liu, and L. H. A. Nay, "Effect of radial magnetic forces in permanent magnet motors with rotor eccentricity", *IEEE Trans. Magn.*, vol. 43, no. 6, pp. 2525-2527, 2007.
- [8] F. B. Alam, B. Rezaeaealam, and J. Faiz, "Unbalanced magnetic force analysis in eccentric surface permanent-magnet motors using an improved conformal mapping method", *IEEE Trans. Energy Convers.*, vol. 32, no. 1, pp. 146-154, 2017.
- [9] L. J. Wu, Z. Q. Zhu, Y. T. Fang, and X. Y. Huang, "Difference in unbalanced magnetic force of fractional-slot PM machines between

internal and external rotor topologies,” *CES Transactions on Electrical Machines and Systems*, vol. 1, no. 2, pp. 154-163, 2017.

- [10] L. J. Wu, Z. Q. Zhu, M. L. M. Jamil, “Unbalanced magnetic force in permanent magnet machines having asymmetric windings and static/rotating eccentricities,” *International Conference on Electrical Machines and Systems (ICEMS)*, 2013.
- [11] Z. Q. Zhu, M. L. M. Jamil, L. J. Wu, “Influence of slot and pole number combinations on unbalanced magnetic force in PM machines with diametrically asymmetric windings,” *IEEE Trans. Ind. Appl.*, vol.49, no.1, pp.1-1, 2013.
- [12] L. J. Wu, Z. Q. Zhu, J. T. Chen, and Z. P. Xia, “An analytical model of unbalanced magnetic force in fractional-slot surface-mounted permanent magnet machines,” *IEEE Trans. Magn.*, vol. 46, no. 7, pp. 2686–2700, Jul. 2010.
- [13] L. J. Wu, Z. Q. Zhu, Y. T. Fang, and X. Y. Huang, “Influence of magnet height on unbalanced magnetic force of surface-mounted permanent magnet machines,” *Vehicle Power and Propulsion Conference (VPPC)*, 2016.
- [14] J. Ma, Z. Q. Zhu, and L. J. Wu, “Influence of slot/pole combination and magnet thickness on unbalanced magnetic force in PM machines with different rotor eccentricities and magnetizations,” *International Conference on Electrical Machines and Systems (ICEMS)*, 2017.
- [15] J. Ma, and Z. Q. Zhu, “Effect of magnet thickness on electromagnetic performance of high speed permanent magnet machines,” *International Conference on Electrical Machines and Drives (IEMDC)*, 2017.
- [16] J. Krotsch, T. Ley, and B. Piepenbreier, “Reduction of torque and radial force fluctuation in permanent magnet synchronous motors by means of multi-objective optimization,” in *Proc. 1st Int. Electr. Drives Prod. Conf. (EDPC)*, Sep. 2011, pp. 40–48.
- [17] G. Jiao and C. D. Rahn, “Field weakening for radial force reduction in brushless permanent-magnet DC motors,” *IEEE Trans. Magn.*, vol. 40, no. 5, pp. 3286–3292, Sep. 2004.
- [18] H. Yang and Y. Chen, “Influence of radial force harmonics with low mode number on electromagnetic vibration of PMSM,” *IEEE Trans. Energy Convers.*, vol. 29, no. 1, pp. 38–45, Mar. 2014.
- [19] G. Jang and D. Lieu, “The effect of magnet geometry on electric motor vibration,” *IEEE Trans. Magn.*, vol. 27, pp. 5202–5204, Nov. 1991.
- [20] G. Jang and D. Lieu, “Vibration reduction in electric machine by interlocking of the magnets,” *IEEE Trans. Magn.*, vol. 29, pp. 1423–1426, Mar. 1993.
- [21] G.-H. Kang, J. Hur, W.-B. Kim, and B.-K. Lee, “The shape design of interior type permanent magnet BLDC motor for minimization of mechanical vibration,” in *Proc. Energy Convers. Congr. Expo.*, Sep. 2009, pp. 2409–2414.
- [22] A. Binder, T. Schneider, and M. Klohr, “Fixation of buried and surface-mounted magnets in high-speed permanent-magnet synchronous machines,” *IEEE Trans. Ind. Appl.*, vol. 42, no. 4, pp. 1031-1037, 2006.
- [23] Y. Pang, and Z. Q. Zhu, “Reduction of unbalanced magnetic force in 2-pole 3-slot permanent magnet machine,” *7th IET Int. Conf. Power Electronics, Machines and Drives (PEMD 2014)*, 2014, pp. 1-6.
- [24] J. Ma, and Z. Q. Zhu, “Unbalanced magnetic force mitigation in 3-slot/2-pole permanent magnet machines by inserting auxiliary slots,” *International Conference on Electrical Machines and Drives (IEMDC)*, 2017.
- [25] W. Q. Chu and Z. Q. Zhu, “Average torque separation in permanent magnet synchronous machines using frozen permeability,” *IEEE Trans. Magn.*, vol. 49, no. 3, pp. 1202–1210, Mar. 2013.



**Z. Q. Zhu (M’90–SM’00–F’09)** received the B.Eng. and M.Sc. degrees from Zhejiang University, Hangzhou, China, in 1982 and 1984, respectively, and the Ph.D. degree from the University of Sheffield, Sheffield, U.K., in 1991, all in electrical engineering.

From 1984 to 1988, he lectured in the Department of Electrical Engineering, Zhejiang University. Since 1988, he has been with the University of Sheffield, where since 2000, he has been a Professor of electrical machines and control systems in the Department of Electronic and Electrical Engineering, and is currently the Head of the Electrical Machines and Drives Research Group, the Royal Academy of Engineering/Siemens Research Chair, Academic Director of Sheffield Siemens Wind Power Research Centre, Director of CRRC Electric Technology Research Centre, Director of Midea Electrical Machines and Controls Research and Development Centres. His current major research interests include the design and control of permanent magnet machines and drives for applications ranging from automotive through domestic appliance to renewable energy. He is a Fellow of the Royal Academy of Engineering, UK.



**Jie Ma** was born in Shanxi, China, in 1992. He received the M.Sc. degree in electronic and electrical engineering from the University of Sheffield, Sheffield, U.K., in 2015. He is currently working toward the Ph.D. degree at the University of Sheffield, Sheffield, U.K.

His major research interests include the design and analysis of high speed permanent magnet machines.